

# Kohn anomalies and non-adiabaticity in doped carbon nanotubes

Nicolas Caudal, A. Marco Saitta,\* Michele Lazzeri, and Francesco Mauri

*Institut de Minéralogie et Physique des Milieux Condensés,  
CNRS-UMR 7590, Université Pierre et Marie Curie-Paris 6,  
Université Denis Diderot-Paris 7, IPGP, F-75252 Paris, France*

(Dated: October 6, 2018)

The high-frequency Raman-active phonon modes of metallic single-walled carbon nanotubes (SWNTs) are thought to be characterized by Kohn anomalies (KAs) resulting from the combination of SWNTs intrinsic one-dimensional nature and a significant electron-phonon coupling (EPC). KAs are expected to be modified by the doping-induced tuning of the Fermi energy level  $\epsilon_F$ , obtained through the intercalation of SWNTs with alkali atoms or by the application of a gate potential. We present a Density-Functional Theory (DFT) study of the phonon properties of a (9,9) metallic SWNT as a function of electronic doping. For such study, we use, as in standard DFT calculations of vibrational properties, the Born-Oppenheimer (BO) approximation. We also develop an analytical model capable of reproducing and interpreting our DFT results. Both DFT calculations and this model predict, for increasing doping levels, a series of EPC-induced KAs in the vibrational mode parallel to the tube axis at the  $\Gamma$  point of the Brillouin zone, usually indicated in Raman spectroscopy as the  $G^-$  peak. Such KAs would arise each time a new conduction band is populated. However, we show that they are an artifact of the BO approximation. The inclusion of non-adiabatic (NA) effects dramatically affects the results, predicting KAs at  $\Gamma$  only when  $\epsilon_F$  is close to a band crossing  $E_X$ . For each band crossing a double KA occurs for  $\epsilon_F = E_X \pm \hbar\omega/2$ , where  $\hbar\omega$  is the phonon energy. In particular, for a 1.2 nm metallic nanotube, we predict a KA to occur in the so-called  $G^-$  peak at a doping level of about  $N_{el}/C = \pm 0.0015$  atom ( $\epsilon_F \approx \pm 0.1$  eV) and, possibly, close to the saturation doping level ( $N_{el}/C \sim 0.125$ ), where an interlayer band crosses the  $\pi^*$  nanotube bands. Furthermore, we predict that the Raman linewidth of the  $G^-$  peak significantly decreases for  $|\epsilon_F| \geq \hbar\omega/2$ . Thus our results provide a tool to determine experimentally the doping level from the value of the KA-induced frequency shift and from the linewidth of the  $G^-$  peak. Finally, we predict KAs to occur in phonons with finite momentum  $\mathbf{q}$  not only in proximity of a band crossing, but also each time a new band is populated. Such KAs should be observable in the double-resonant Raman peaks, such as the defect-activated  $D$  and peak, and the second-order peaks  $2D$  and  $2G$ .

PACS numbers: 73.63.Fg, 71.15.Mb, 63.20.Kr, 78.67.Ch

## I. INTRODUCTION

Since their discovery in 1991<sup>1</sup>, carbon nanotubes have raised an enormous interest both from the academic and the technological points of view. They exhibit in fact a variety of exciting features: their quasi-one-dimensional nature, due to a diameter of 1-2 nm and a length of up to several micrometers, makes them sharp probes for scanning tunneling microscopes and an excellent model for one-dimensional physics. Their mechanical and tensile strength make them of great interest in composite materials, and, most significantly of all, they have very unusual and extremely promising electronic properties, displaying metallic or semiconducting behavior according to their structure and helicity<sup>2,3</sup>. The electronic properties of SWNTs, already particularly interesting from the technological point of view, promise to be the future of nano-electronics due to their *tunability*, achieved by doping the nanotubes through intercalation with alkali atoms<sup>4,5,6,7,8,9,10,11,12,13</sup> or application of a gate potential<sup>14,15,16,17</sup>. However, there are still a number of experimental challenges to be solved in order to fully develop SWNT-based nano-electronic technology, in particular the low-cost industrial-scale synthesis of nanotubes of good chemical purity, crystalline quality and given helicity.

An experimental tool largely used to characterize SWNTs is Raman spectroscopy<sup>4,5,6,7,8,9,15,16,17,18,19,20,21,22,23</sup>. Typical Raman spectra of carbon nanotubes display a peak around 150-300  $cm^{-1}$ , due to the radial breathing mode (RBM), which

has been recently used as a tool to infer the size and chirality of the nanotubes<sup>20,23</sup>. Other important features of SWNT Raman spectra include a peak around 1350  $cm^{-1}$ , activated by defects and impurities, and known in the literature as  $D$  peak, and a large structure around 1570  $cm^{-1}$ , due to modes tangential to the nanotube and known as  $G$  peak. This last feature is thought to have two components, usually referred to as  $G^+$  and  $G^-$ , originating from the  $E_{2g}$  in-plane modes of graphite. In refs.<sup>24,25,26</sup> it has been shown that in metallic SWNTs the  $G^+$  component corresponds to the tangential vibrational mode *perpendicular* to the nanotube axial direction, while the  $G^-$  component corresponds to the tangential vibrational mode *parallel* to the nanotube axial direction. In the following, we will refer to the former as “the nanotube TO tangential mode”, and to the latter as “the nanotube LO axial mode”. Some Raman studies<sup>5,6,7,8</sup> show that the frequency of the  $G$  peak increases up to 1600  $cm^{-1}$  at low doping levels, and then suddenly drops to about 1550  $cm^{-1}$  at the saturation threshold of alkali intercalation, estimated around a number of electrons per carbon atom  $N_{el}/C = 0.12$  (MC<sub>8</sub>).

Other experimental<sup>9,16,18</sup> and theoretical<sup>27,28,29</sup> works on the effect of doping on SWNTs report a similar  $G$ -peak softening or even a Luttinger-Fermi liquid transition<sup>12</sup>. Since the LO axial and TO tangential modes are particularly sensitive to the electronic structure of SWNTs around the Fermi energy<sup>24,26,27,30,31</sup>  $\epsilon_F$ , and  $\epsilon_F$  directly depends on the charge doping level, a profound understanding of the interplay between the

vibrational and the electronic properties of nanotubes looks to be crucial for technological development.

In this work we report our theoretical study of the electronic and vibrational properties of doped SWNTs, based on DFT first-principles calculations and analytical results. We will show in the following that: *i*) the vibrational properties of SWNTs can be obtained from the so-called *electronic zone-folding* of a graphene sheet; *ii*) their behavior as a function of the charge doping level can be determined by the knowledge of electron-phonon coupling (EPC) in graphene; *iii*) ordinary quantum-mechanics calculations relying on the adiabatic Born-Oppenheimer approximation fail when applied to SWNTs, where non-adiabatic effects are enhanced by their intrinsic one-dimensional nature.

Our paper is organized as follows: in section II we will describe our theoretical framework, and in particular how the Raman-active modes of a nanotube can be accurately obtained through an appropriate electronic sampling of the graphene Brillouin Zone (BZ). We will then show in section III that the DFT results can be almost perfectly reproduced by an integral model, that uses the graphite EPC and the slope of the electronic bands around the (undoped) Fermi level  $\epsilon_F^0$  (usually referred to as the  $\pi$  and  $\pi^*$  bands) as external inputs, and that becomes analytical in the limit of vanishing temperature. The results on the DFT and the model-derived LO axial and TO tangential modes of a SWNT will be presented, showing that Kohn anomalies (KA) would occur, within the adiabatic approximation, each time a new electronic band is populated by the electrons at  $\epsilon_F$ . In section IV we show that when the Born-Oppenheimer approximation is lifted the outcome is dramatically different, and that a drop in the frequency of the  $G^-$  peak occurs at a doping level such that  $\epsilon_F - \epsilon_F^0 \approx 0.1$  eV or close to the saturation level. Section V will be devoted to the discussion of the physical properties of metallic SWNTs that are experimentally accessible, and to the conclusions.

## II. THEORETICAL BACKGROUND

### A. General description of graphene and SWNTs

Graphene is a semimetal, and its highest valence and lowest conduction bands have a circular conical surface shape around the points  $\mathbf{K}$  and  $\mathbf{K}'$  of the hexagonal first Brillouin zone at zero doping; its Fermi surface is reduced to the vertexes of the cones at those two points.

The structure of a SWNT is obtained by rolling a sheet of 2D graphene, and closing both ends with fullerene-like semi-spheres. However, nanotubes are commonly studied as infinite 1D crystals, *i.e.* neglecting the details of those ends. Nanotubes are then uniquely determined by the knowledge of the chiral vector  $\mathbf{C}_h = n\mathbf{a}_1 + m\mathbf{a}_2$ , where  $\mathbf{a}_1$  and  $\mathbf{a}_2$  are the basis vectors of graphene,  $n$  and  $m$  are integers<sup>2,3</sup>. The translational vector determines the periodicity along the tube axis and is  $\mathbf{T} = \frac{(2m+n)}{d_R}\mathbf{a}_1 - \frac{(2n+m)}{d_R}\mathbf{a}_2$ , where  $d_R$  is the greatest common divisor of  $(2m+n)$  and  $(2n+m)$ . Nanotubes with indexes such that  $n-m=3k$ , where  $k$  is an integer, are metallic, otherwise they are semiconductors. Nanotubes with

identical indexes, *i.e.*  $n=m$ , are thus always metallic, and are usually called ‘‘armchair’’ tube.

Electronic zone folding (EZF) is a common approximation for the electronic band structure of a SWNT, which consists in neglecting the curvature of the SWNT. Within the EZF the electronic states of a SWNT are approximated by the electronic states of a graphene sheet having wavevector  $\mathbf{k}$  such that  $\mathbf{k} \cdot \mathbf{C}_h = 2\pi\nu$ , being  $\nu$  an integer. The wave-vectors allowed for the SWNT satisfy

$$\mathbf{k} = \nu\mathbf{k}_\perp + k\mathbf{k}_\parallel / \|\mathbf{k}_\parallel\| \quad (1)$$

where  $k$  is a real,  $\mathbf{k}_\parallel$  is parallel to the tube axis,  $\mathbf{k}_\perp$  is perpendicular to the tube axis and satisfies  $\|\mathbf{k}_\perp\| = 2\pi/\|\mathbf{C}_h\| = 2/d$ ,  $d$  being the tube diameter.

This way of constructing the electronic band structure accounts for the fact that SWNTs can be either metallic or semiconducting. In fact, if in SWNTs a line of allowed wave vectors  $\mathbf{k}$  crosses the  $\mathbf{K}$  or the  $\mathbf{K}'$  point, the nanotube is metallic, otherwise it is a semiconductor. In particular, in the BZ of armchair metallic SWNTs the section of the vertical plane containing the  $\nu = 0$  line of  $\mathbf{k}$  vectors and the conical bands consists of two straight lines of slope  $\pm\beta$ , while the conic sections for  $|\nu| \geq 1$  consist of arms of hyperbolae. The energy difference between the maximum of the lower arm and the minimum of the upper arm are usually indicated as  $E_{\nu\nu}^M$  in the metallic case (see also Fig. 2).

Previous works<sup>2,3,24,25,32</sup> have shown that the effects of the nanotube curvature can be neglected as a first approximation for SWNTs whose diameter is larger than 1 nm (the most common nanotubes present in experimental samples) and the electronic properties of a nanotube can be quite accurately obtained from EZF.

### B. Electronic zone-folding for phonon calculations

The explicit calculation of the full dynamical matrix of an infinite nanotube, even within an efficient scheme such as Density-Functional Perturbation Theory (DFPT)<sup>33</sup>, is a quite demanding task from the computational point of view. On the other hand, the SWNT vibrational modes typically observed in Raman spectra can be traced back to the phonon and elastic modes of an isolated graphene sheet.

However, it has been shown that the phonon dispersions of SWNTs cannot be as accurately reconstructed from the graphene ones as the electronic bands, because of the presence of KAs which behave differently in graphene<sup>34</sup> and metallic SWNTs<sup>24,25,26,27,30,31</sup>. The KAs are determined by singularities in the electron screening and such singularities depends on the dimensionality of the electron Brillouin zone. The dimensionality is two for graphene and one for SWNTs. This reduced SWNT dimensionality is due to the quantization (*confinement*) of the electronic wavevector around the nanotube circumference, which is actually described by the EZF. This last consideration suggests a practical scheme for the calculation of the phonon dispersion in SWNTs which neglects curvature, but fully takes into account the more important confinement effects. Phonons in nanotubes are well approximated

by the phonons of a flat graphene sheet, if the calculation is done performing the electronic Brillouin-zone integration on the lines of the electronic zone-folding (Eq. 1). Such phonon calculation method (phonon-EZF) was introduced in refs.<sup>24,25</sup>. A phonon-EZF calculation requires the use of a unit cell containing two atoms and thus, is clearly much less computationally demanding than full calculations on an actual SWNT, which requires a unit-cell with tens or hundreds of atoms. In Subsect. IID we will demonstrate that, for the preset study, curvature effects are negligible and the phonon-EZF provides an accurate description of the high-frequency phonon modes.

### C. Computational details

Our first-principles calculations are based on DFT, within the plane-wave (PW)/pseudopotential scheme implemented in the Quantum-ESPRESSO code<sup>35</sup>. We adopt a Perdew-Burke-Erzerhof gradient corrected functional, and an ultrasoft pseudopotential to describe the  $C$  atom. A PW kinetic energy cut-off of 30 Ry is sufficient to ensure convergence on the structural, electronic, and vibrational properties. We choose as a case-study the (9,9) metallic armchair SWNT, containing 36 distinct carbon atoms, and having a tube diameter of 1.24 nm. The full nanotube calculations are performed by setting the nanotube in an infinite lattice of hexagonal symmetry in the plane perpendicular to the tube axis, mimicking thus the bulk effect of a real nanotube bundle or an isolated tube by tuning the lattice parameter between 1.56 nm and 1.72 nm. The  $c$  axis is maintained constant. Integrations in the nanotube one-dimensional Brillouin zone have been performed by using regular grids of  $\mathbf{k}$  points along the  $c$  reciprocal axis. We use a Fermi-Dirac electronic smearing of 0.01 Ry (corresponding to an electronic temperature of 1578 K) for SWNT full phonon calculations, and of 0.002 Ry (315 K) for structural calculations and frozen-phonon tests (see below). Grids of 8 and 40  $\mathbf{k}$  points were sufficient, respectively, to ensure a good convergence ( $\sim 5 \text{ cm}^{-1}$ ) on the LO axial frequencies in the two cases.

In the phonon-EZF calculation we use a graphene hexagonal unit cell of lattice parameter  $a_{\text{exp}} = 2.47 \text{ \AA}$  and  $c = 5 \text{ \AA}$ . The number of points is chosen as to ensure phonon frequencies converged within about  $0.3 \text{ cm}^{-1}$ , and is inversely proportional to temperature. At a temperature of 315 K, the total number of points is 3240, equivalent to 180 points along the  $c$  direction of the reciprocal space of the (9,9) nanotube, while at 1578 K this number reduces to 720, equivalent to 40 points in the nanotube case. For both the full nanotube and the phonon-EZF case, the effect of (low) charge doping is simulated by adding an excess electronic charge which is compensated by a uniformly charged background. This is done using the standard implementation of the ESPRESSO-package<sup>35</sup>. This approach is known to describe very well the properties of doped SWNTs<sup>36</sup>. This is justified even in the case of alkali intercalation by the report that at low doping levels, *i.e.* up to MC<sub>15</sub>, the electronic charge of the metal atoms is thought to be completely transferred<sup>37</sup>, and that the effect of the intercalation is essentially described by taking into account the sole effect of

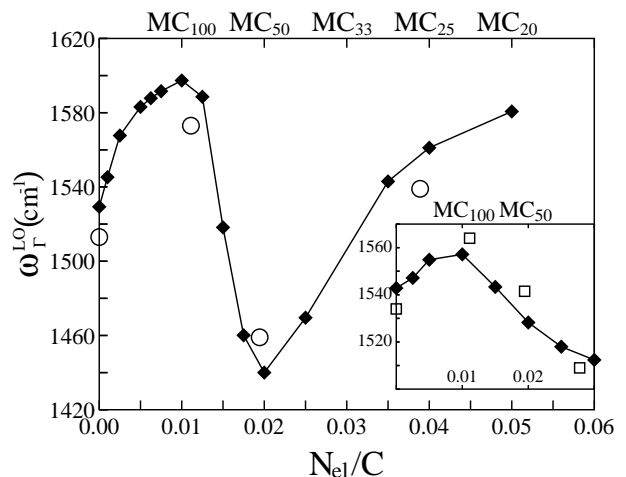


FIG. 1: Variation of the LO axial frequencies with electron doping at 315 K, calculated from phonon-EZF (full diamonds) or through full-nanotube frozen-phonon (open circles). The solid line is a guide to the eye. The metal/carbon composition corresponding to the doping level is indicated on the top of the figure. Inset: variation with electronic doping of the phonon-EZF LO axial frequency (full diamonds) compared to a SWNT full DFPT dynamical matrix calculation (open squares), at 1578 K.

the charge transfer.

### D. Accuracy of the method of phonon calculation

The first step of our study is to assess the accuracy of the phonon-EZF method with respect to the SWNT phonon calculations. In Fig. 1 we show the frequency of the LO axial mode as a function of electronic doping at 315 K, obtained both through the phonon-EZF method or by an explicit nanotube frozen-phonon calculation. In the latter case, the atoms are displaced along the axial direction of the nanotube, and the frequency is obtained by the curvature of the displacement energy. The convergence of this single-mode frozen-phonon frequency has been confirmed by testing the result with a more accurate sampling of the BZ, that is up to 200 uniformly-spaced  $\mathbf{k}$  points in the one-dimensional BZ grid. In the inset we analogously compare the phonon-EZF LO axial frequency with a full DFPT nanotube phonon calculation at 1578 K. In this latter case, all the 108  $\Gamma$  vibrational modes of the nanotube are explicitly calculated; a lower temperature, and thus a correspondingly larger grid of at least 40  $\mathbf{k}$  points, would be computationally too demanding for a complete and accurate study of the problem. Both graphs show that phonon-EZF not only determines the nanotube phonon frequencies in good agreement with explicit SWNT calculations, but it also captures very well the strikingly non-monotonic dependence of the LO axial mode with respect to electronic doping, to be discussed later on, confirming that the effects of the SWNT curvature can be confidently neglected for a (9,9) armchair nanotube, and that phonon-EZF is a reliable and accurate method.

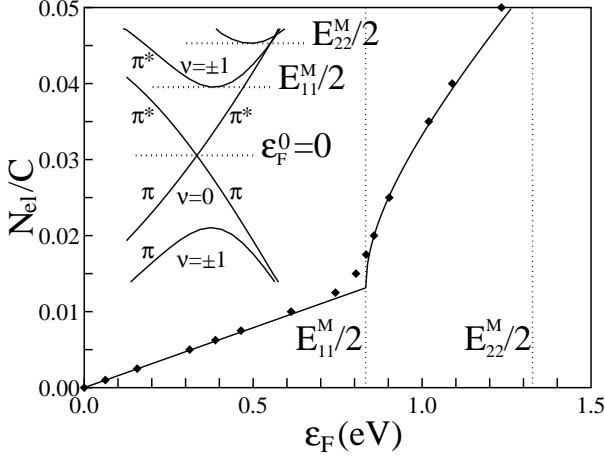


FIG. 2: Variation of the electronic doping per  $C$  atom as a function of the Fermi energy  $\epsilon_F$ . Solid line: analytical expression (Eq.2) with  $E_{11}^M/2 = 0.83$  eV; diamonds: DFT calculations, within phonon-EZF, of the Fermi energy in a (9,9) SWNT at 315 K. The  $E_{11}^M/2$  and  $E_{22}^M/2$  levels are indicated by vertical dotted lines. Inset: Calculated electronic bands of the (9,9) SWNT around the  $\mathbf{K}$  point.  $\epsilon_F^0$  is taken as the zero energy,  $E_{11}^M/2$  and  $E_{22}^M/2$  are the minima of the second and third (hyperbolic) conduction bands. The valence bands (below  $\epsilon_F^0$ ) and the conduction bands (above  $\epsilon_F^0$ ) are usually referred to as the  $\pi$  and  $\pi^*$  bands, respectively. The bands crossing at  $\epsilon_F^0$  have the index  $\nu = 0$ , while the valence and conduction bands immediately below and above have indexes  $\nu = \pm 1$  (see Eq. 1).

### E. Fermi level in doped SWNTs

The key quantity intervening in the anomalous vibrational properties of SWNTs is the Fermi energy level  $\epsilon_F$ . In undoped graphene and in metallic armchair nanotubes, its value ( $\epsilon_F^0$ ) coincides with the band energy at the crossing of the  $\pi$  and  $\pi^*$  bands at the  $\mathbf{K}$  and  $\mathbf{K}'$  points of the graphene BZ, and is chosen as the zero band energy hereafter. Since the results are independent on the sign of  $\epsilon_F$ , we consider here and in the following that  $\epsilon_F > 0$ , without loss of generality. Following the description of the graphene electronic bands in terms of conic sections as in subsection II A, the increase of  $\epsilon_F$  due to electronic doping per carbon atom  $N_{el}/C$  in a  $(n, n)$  SWNT can be analytically expressed, at low doping levels and a temperature  $T=0$  K, by the following formula:

$$N_{el}/C(\epsilon_F) = \frac{a_0^2 \sqrt{3}}{\pi \beta d} \epsilon_F + \theta(\epsilon_F - E_{11}^M/2) \frac{2a_0^2 \sqrt{3}}{\pi \beta d} \sqrt{\epsilon_F^2 - (E_{11}^M/2)^2} \quad (2)$$

where  $a_0$  is the lattice parameter,  $\beta$  is the slope of the conical bands and equals  $14.1$  eV  $\frac{a_0}{2\pi}$ , and  $\theta(x)$  is the step function. As previously mentioned, the energies of electronic transitions in SWNTs are usually indicated as  $E_{ii}^{M/S}$ , where, for armchair SWNTs,  $i$  coincides with the  $\nu$  band index of the initial and final states, and the superscript refers to metallic or semiconducting SWNTs. In the case of a  $(n, n)$  nanotube, assuming perfect conical bands,  $E_{11}^M/2 = 2\beta/d$ . In particular, for the (9,9) nanotube  $E_{11}^M/2 = 0.89$  eV.

We report in Fig. 2 the corresponding curve relating  $\epsilon_F$  to  $N_{el}/C$ , along with our DFT calculations at 315 K. The most significant discrepancy being between the ideal value of  $E_{11}^M/2$  and the calculated one, which is  $0.83$  eV. If however we treat  $E_{11}^M/2$  as an independent parameter, and we red-shift it by  $0.06$  eV, the agreement is very good. This indicates that the analytical expressions can be safely used to develop an integral and analytical model, based on the EPC and the electronic bands, aimed at describing and predicting the behavior of the LO axial and TO tangential modes in metallic nanotubes. The electronic bands of the nanotube, explicitly calculated by DFT, are shown in the inset around the  $\mathbf{K}$  point of the BZ, along with the band nomenclature  $\pi/\pi^*$ ,  $\nu$  used in the literature and adopted in this work. One can notice that the minimum of the  $\nu = \pm 1$  conduction band is slightly displaced to the right, and that the bands deviate from the conical shape far from  $\mathbf{K}$ . In the following we will use a polynomial fit of the calculated bands in numerical evaluation of integral expressions, while the ideal conical shape of the bands will be used to determine the analytical limits at low temperature.

## III. INTEGRAL AND ANALYTICAL MODEL

### A. Electron-phonon coupling contribution to the dynamical matrix

The frequency of a vibrational mode at a  $\mathbf{q}$  wavevector, is obtained from the dynamical matrix  $D_{\mathbf{q}}$

$$\omega_{\mathbf{q}} = \sqrt{\frac{D_{\mathbf{q}}}{M}}, \quad (3)$$

where  $M$  is the atomic mass of carbon. As shown in refs.<sup>25,34</sup>, the dynamical matrix can be written as the sum of an EPC direct contribution  $\tilde{D}_{\mathbf{q}}$ , which contains non-analytical terms giving rise to Kohn anomalies, and a term containing all the other contributions:

$$D_{\mathbf{q}} = \tilde{D}_{\mathbf{q}} + D_{\mathbf{q}}^{\text{other}} \quad (4)$$

The direct contribution of EPC to the dynamical matrix can be written as

$$\tilde{D}_{\mathbf{q}} = \frac{2}{N_{\mathbf{k}}} \sum_{\mathbf{k}, i, f} \frac{f(\epsilon_{\mathbf{k}, i}) - f(\epsilon_{\mathbf{k}+\mathbf{q}, f})}{\epsilon_{\mathbf{k}, i} - \epsilon_{\mathbf{k}+\mathbf{q}, f}} \cdot |G_{(\mathbf{k}+\mathbf{q}), f; \mathbf{k}, i}|^2 \quad (5)$$

where  $N_{\mathbf{k}}$  is the number of points in the SWNT Brillouin zone,  $i$  and  $f$  are the band indexes indicating the two states involved in the electronic transition. Since we consider only the contribution of the  $\pi$  and  $\pi^*$  bands,  $i, f = \pi, \pi^*$ . The function  $f(\epsilon) = \{\exp[(\epsilon - \epsilon_F)/kT] + 1\}^{-1}$ , is the Fermi-Dirac distribution;  $G_{(\mathbf{k}+\mathbf{q}), f; \mathbf{k}, i}$  is the EPC matrix element, defined as

$$G_{(\mathbf{k}+\mathbf{q}), f; \mathbf{k}, i} = \langle \mathbf{k} + \mathbf{q}, f | \Delta V_{\mathbf{q}} | \mathbf{k}, i \rangle \quad (6)$$

where  $\Delta V_{\mathbf{q}}$  is the first-order derivative of the Kohn-Sham self-consistent potential with respect to the atomic displacements corresponding to a  $\mathbf{q}$ -vector phonon;  $|\mathbf{k}, i\rangle$  is the Bloch

electronic wavefunction. Hereafter, we develop our model on the basis of the EZF sampling, and the  $\mathbf{k}$  vectors are those allowed by Eq. 1. Since we study phonons close to  $\Gamma$  we limit ourselves to wave vectors entirely along  $\mathbf{k}_{\parallel}$  writing  $\mathbf{q} = q\mathbf{k}_{\parallel}/\|\mathbf{k}_{\parallel}\|$  and  $\|\mathbf{q}\| \ll \|\mathbf{K}\|$ . Therefore  $\nu$  is conserved through the transition  $i \rightarrow f$ . In the limit of a nanotube of infinite length we replace  $\frac{1}{N_{\mathbf{k}}}\sum_{\mathbf{k}}$  by  $\sum_{\nu}\frac{T}{2\pi}\int dk$ , which yields for the non-analytical part of the dynamical matrix

$$\tilde{D}_{\mathbf{q}} = \frac{T}{\pi} \sum_{\nu,i,f} \int dk \frac{f[\epsilon_{\nu,i}(k)] - f[\epsilon_{\nu,f}(k+q)]}{\epsilon_{\nu,i}(k) - \epsilon_{\nu,f}(k+q)} \cdot |G_{(\mathbf{k}+\mathbf{q}),f;\mathbf{k},i}|^2 \quad (7)$$

Neglecting the effects of curvature, the EPC matrix element  $G_{(\mathbf{k}+\mathbf{q}),f;\mathbf{k},i}$  of a nanotube of diameter  $d$  and longitudinal period  $T$  is related to the EPC  $\tilde{G}_{(\mathbf{k}+\mathbf{q}),f;\mathbf{k},i}$  of graphene by the ratio of the unit cells areas (Eq.4 of<sup>38</sup>):

$$d\pi T |G_{(\mathbf{k}+\mathbf{q}),f;\mathbf{k},i}|^2 = \frac{a_0^2\sqrt{3}}{2} |\tilde{G}_{(\mathbf{k}+\mathbf{q}),f;\mathbf{k},i}|^2 \quad (8)$$

The main contribution to the EPC term originates from the  $\mathbf{K}$  point of the graphene BZ, so we can define the wavevector  $\mathbf{k}' = \mathbf{k} - \mathbf{K}$ . Furthermore, since KAs originate when the denominator in Eq. 7 vanishes, we can restrict the integral in the BZ to a small interval of width  $2\bar{k}$  around  $\mathbf{K}$  (and  $\mathbf{K}'$ ). We can also define the angles  $\theta$ , between  $\mathbf{k}'$  and  $\mathbf{q}$ , and  $\theta'$ , between  $\mathbf{k}' + \mathbf{q}$  and  $\mathbf{q}$ . In refs.<sup>24,34</sup> it was shown that for phonons close to  $\Gamma$ , the nanotube EPC can be in principle expressed in terms of the graphene EPC  $\langle G_{\Gamma}^2 \rangle_{\text{F}} = 45.60 \text{ (eV/\AA)}^{234}$ , modulated by a geometric factor:

$$|\tilde{G}_{(\mathbf{k}+\mathbf{q}),f;\mathbf{k},i}^{\text{TO/LO}}|^2 = \langle G_{\Gamma}^2 \rangle_{\text{F}} [1 \pm \text{sign}(\epsilon_{\nu,f} \cdot \epsilon_{\nu,i}) \cos(\theta + \theta')] \quad (9)$$

where

$$\cos(\theta + \theta') = \frac{k'(k' + q) - (\nu k_{\perp})^2}{\sqrt{k'^2 + (\nu k_{\perp})^2} \sqrt{(k' + q)^2 + (\nu k_{\perp})^2}} \quad (10)$$

and the  $+$ ( $-$ ) sign has to be considered for TO tangential(LO axial) modes. This expression, developed through a first-neighbor tight-binding model was then quantitatively confirmed by direct DFT calculations<sup>34</sup>. The TO tangential/LO axial terms of the non-analytical part of the dynamical matrix can thus be written as:

$$\tilde{D}_{\mathbf{q}}^{\text{TO/LO}} = \frac{a_0^2\sqrt{3}\langle G_{\Gamma}^2 \rangle_{\text{F}}}{\pi^2 d} \sum_{\nu,f,i} \int_{-\bar{k}}^{\bar{k}} dk' \frac{f[\epsilon_{\nu,i}(k')] - f[\epsilon_{\nu,f}(k'+q)]}{\epsilon_{\nu,i}(k') - \epsilon_{\nu,f}(k'+q)} \cdot [1 \pm \text{sign}(\epsilon_{\nu,f} \cdot \epsilon_{\nu,i}) \cos(\theta + \theta')] \quad (11)$$

where a factor 2 is included to take into account the contribution of the two equivalent points  $\mathbf{K}$  and  $\mathbf{K}'$ .

Since we are interested in phonons close to  $\Gamma$ , we should consider the  $\mathbf{q} \rightarrow 0$  limit in Eq. 11:

$$\tilde{D}_{\Gamma}^{\text{TO/LO}} = \frac{a_0^2\sqrt{3}\langle G_{\Gamma}^2 \rangle_{\text{F}}}{\pi^2 d} \int_{-\bar{k}}^{\bar{k}} dk' \left\{ \sum_{\nu,f \neq i} \frac{f[\epsilon_{\nu,i}(k')] - f[\epsilon_{\nu,f}(k')]}{\epsilon_{\nu,i}(k') - \epsilon_{\nu,f}(k')} \cdot [1 \pm \text{sign}(\epsilon_{\nu,f} \cdot \epsilon_{\nu,i}) \cos(2\theta)] + \sum_{\nu,f} \frac{\partial f}{\partial \epsilon} [\epsilon_{\nu,f}(k')] \cdot [1 \pm \cos(2\theta)] \right\} \quad (12)$$

where we distinguish between *interband* ( $i \neq f$ , first line) and *intra-band* ( $i = f$ , second line) transitions, for which we used the following limit:

$$\lim_{\mathbf{q} \rightarrow 0} \frac{f[\epsilon_{\nu,f}(k')] - f[\epsilon_{\nu,f}(k'+q)]}{\epsilon_{\nu,f}(k') - \epsilon_{\nu,f}(k'+q)} = \frac{\partial f}{\partial \epsilon} [\epsilon_{\nu,f}(k')]. \quad (13)$$

Then if the temperature  $T \rightarrow 0$ ,

$$\frac{\partial f}{\partial \epsilon} [\epsilon_{\nu,f}(k')] = -\frac{4\pi^2 d}{\sqrt{3}a_0^2} \sum_{\sigma=\pm} DOS_{\nu,f,\sigma}(\epsilon_F) \delta(k' - k_{\nu,f,\sigma}^F) \quad (14)$$

where  $DOS_{\nu,f,\sigma}(\epsilon_F)$  and  $k_{\nu,f,\sigma}^F$  are the electronic *density of states* (DOS) per  $C$  atom and the Fermi wavevector of the  $f$  band of  $\nu$  index and slope of sign  $\sigma$ . The intraband EPC contribution to the dynamical matrix at  $\Gamma$  is thus proportional to the density of states at the Fermi level.

The dynamical matrix at finite  $\mathbf{q}$  can be calculated by using the general expression (11); in the following we will focus on the contribution at  $\mathbf{q}=0$  of the lowest conduction band  $\nu=0$ ,  $\tilde{D}_{\Gamma}^0$ , and the second lowest bands  $\nu = \pm 1$ ,  $\tilde{D}_{\Gamma}^{\pm 1}$ , as functions of the Fermi energy

$$\tilde{D}_{\Gamma}(\epsilon_F) = \tilde{D}_{\Gamma}^0(\epsilon_F) + \tilde{D}_{\Gamma}^{\pm 1}(\epsilon_F) \quad (15)$$

The contribution of higher conduction bands could be in principle included with no difficulty in the same form as the  $\nu = \pm 1$  bands, but their effect is negligible for the doping levels considered in this work, up to  $N_{el}/C \sim 0.06$ , *i.e.* the value of estimated total charge transfer in the case of alkali intercalation<sup>37</sup>.

## B. Contribution of the $\nu = 0$ bands

The bands intersecting at the  $\mathbf{K}$  point of the graphene BZ are at a good approximation linear around  $\mathbf{K}$ , as shown in the previous section, with slopes  $\pm\beta = 14.1 \cdot \frac{a_0}{2\pi} \text{ eV}$ . For these branches,  $\nu = 0$ , so that the geometric contribution  $1 \pm \cos(\theta + \theta')$  equals 0 or 2. In practice, in the LO axial case it equals 2 when the transition involves *interband* states with opposite slope, and vanishes for the *intra-band* transitions; the opposite behavior occurs in the TO tangential case<sup>38</sup>. For LO axial

$$\tilde{D}_{\Gamma}^{\text{LO},0} = \frac{2a_0^2\sqrt{3}}{\pi^2 d} \langle G_{\Gamma}^2 \rangle_{\text{F}} \int_{-\bar{k}}^{\bar{k}} dk' \left[ \frac{f(\beta k') - f(-\beta k')}{\beta k'} \right] \quad (16)$$

In the limit  $T \rightarrow 0$ , one obtains

$$\tilde{D}_{\Gamma}^{\text{LO},0} = \frac{4a_0^2\sqrt{3}}{\pi^2 d\beta} \langle G_{\Gamma}^2 \rangle_{\text{F}} \ln \left| \frac{\epsilon_F}{|\beta \bar{k}|} \right| \quad (17)$$

The quantitative result depends on the value of  $\bar{k}$ , which enters the additive constant defined for  $\omega_{LO}$  at the end of the next subsection. Since the density of states is independent of energy for the  $\nu = 0$  band, the non-analytical direct EPC

contribution to the TO tangential mode is also a constant, independent of  $\epsilon_F$

$$\tilde{D}_\Gamma^{\text{TO},0} = -\frac{4a_0^2\sqrt{3}}{\pi^2 d\beta} \langle G_\Gamma^2 \rangle_F \quad (18)$$

which we include in the additive constant defined for  $\omega_{TO}$ . In other words, our model predicts, in the limit of low temperatures, a logarithmic divergence of the dynamical matrix at  $\Gamma$  for zero doping in the LO axial case, while the TO tangential modes are simply red-shifted by the non-analytical EPC contribution.

### C. Contribution of the $\nu = \pm 1$ bands

Let us now consider the second lowest  $\nu = \pm 1$  bands. Since there is a large gap  $E_{11}^M$  between the  $\pi$  and  $\pi^*$  bands, the interband transitions cannot give rise to KAs, and are expected to contribute negligibly to the Fermi level dependence of the phonon frequencies. On the other hand, in the case of doped nanotubes where the  $\nu = \pm 1$  band is partly populated, *intra*band transitions involve a density of states which diverges in one dimension, leading to possible Kohn anomalies. We develop the following analytical expressions based on the ideal hyperbolic  $\nu = \pm 1$  bands. According to Eqs. 12, 13, and 14, the contribution of intraband transitions to  $\tilde{D}_\Gamma$  amounts to

$$\tilde{D}_\Gamma^{\text{TO/LO},1} = -8 \langle G_\Gamma^2 \rangle_F \text{DOS}_{1,\pi^*}(\epsilon_F) \cdot [1 \pm \cos(2\theta_F)] \quad (19)$$

where the  $\nu \pm 1$  degeneracy is taken into account by a factor of 2, and

$$\text{DOS}_{1,\pi^*}(\epsilon_F) = \theta(\epsilon_F - E_{11}^M/2) \frac{2a_0^2\sqrt{3}}{\pi\beta d} \frac{\epsilon_F}{\sqrt{\epsilon_F^2 - (E_{11}^M/2)^2}} \quad (20)$$

is the total DOS of the  $\nu = 1, \pi^*$  band (see Eq. 2). The angular factor at the Fermi wavevector is

$$\cos(2\theta_F) = \frac{(k_{1,\pi^*}^F)^2 - k_\perp^2}{(k_{1,\pi^*}^F)^2 + k_\perp^2} \quad (21)$$

where  $k_{1,\pi^*}^F = \pm \frac{1}{\beta} \sqrt{\epsilon_F^2 - (E_{11}^M/2)^2}$  is the Fermi momentum of the  $\nu = 1, \pi^*$  band. We can notice that the EPC direct contribution  $\tilde{D}_\Gamma^{\text{LO},1}$  is proportional to the density of states of the  $\nu = \pm 1$  conduction bands at the Fermi energy, modulated by the cosine factor. Kohn anomalies would thus occur *where the density of states diverges*. With a few algebraic calculations one obtains, for LO axial phonons, the compact form:

$$\tilde{D}_\Gamma^{\text{LO},1} = -\frac{8a_0^2\sqrt{3}}{\pi^2 d\beta} \langle G_\Gamma^2 \rangle_F \frac{(E_{11}^M/2)^2}{\epsilon_F \sqrt{\epsilon_F^2 - (E_{11}^M/2)^2}} \cdot \theta(\epsilon_F - E_{11}^M/2) \quad (22)$$

For TO tangential modes through similar calculations one finally obtains:

$$\tilde{D}_\Gamma^{\text{TO},1} = -\frac{8a_0^2\sqrt{3}}{\pi^2 d\beta} \langle G_\Gamma^2 \rangle_F \frac{\sqrt{\epsilon_F^2 - (E_{11}^M/2)^2}}{\epsilon_F} \cdot \theta(\epsilon_F - E_{11}^M/2) \quad (23)$$

In this latter case, the divergence of the DOS is canceled by the cosine factor, which equals 0 for  $\epsilon_F = E_{11}^M/2$ . In the following subsection, we will thus calculate through this model the  $\Gamma$  frequency of the TO/LO modes as:

$$\omega_\Gamma^{\text{TO/LO}} = \sqrt{(\omega_\Gamma^{\text{TO/LO,other}})^2 + \frac{\tilde{D}_\Gamma^{\text{TO/LO},0} + \tilde{D}_\Gamma^{\text{TO/LO},1}}{M}}, \quad (24)$$

where  $\omega_\Gamma^{\text{TO/LO,other}} = \omega_\Gamma + C^{\text{TO/LO}}$  contains the unperturbed value  $\omega_\Gamma = 1581 \text{ cm}^{-1}$ , plus an additive constant  $C^{\text{TO/LO}}$ , which also includes the terms discussed at the end of the previous subsection, and is chosen as to match the DFT phonon-EZF results at zero doping; its numerical value, for  $\bar{k} = 0.1 \frac{2\pi}{a_0}$ ; is  $15.1/39.1 \text{ cm}^{-1}$  in the TO/LO case respectively.

### D. Results: Kohn anomalies within the adiabatic approximations

At this point, the actual determination of the effect of EPC in the vibrational properties of doped nanotubes can be in principle carried out by adopting approximated calculation schemes. The DFT phonon calculation of a SWNT is very demanding and is doable only at a relatively high electronic temperature, where the potentially interesting behaviors are smeared out. However, the comparison of the calculations done on a real SWNT with those done using the phonon-EZF (Fig. 1) shows that a quantitative determination of the phonon frequency can be done neglecting the nanotube curvature. Now, we will analyze an integral model which takes another step in identifying the key role played by graphene-derived EPC in the vibrational properties of SWNTs, and its low-temperature limit can be put into an analytical expression. We report in Fig. 3 the frequencies of the LO axial and the TO tangential modes of the  $G$  peak at an electronic temperature of 315 K as a function of the Fermi energy, and thus of the electronic doping, as calculated *i)* from the phonon-EZF method; *ii)* from the numerical integration of Eq. 11 at T=315 K (polynomial fits are used to describe the electronic bands); *iii)* from its analytical limit at T=0 K, where we use the ideal conical bands (Eqs. 17, 18, 22, 23, and 24), with  $E_{11}^M/2$  red-shifted by 0.06 eV as explained in subsection II E.

A first inspection of the graphs indicates that the agreement within the different approaches, and in particular between the DFT calculations and the integral model, is excellent. The LO axial frequency drops at  $\epsilon_F = 0$  due to a Kohn anomaly arising from the first conduction band, and  $\tilde{D}_\Gamma^{\text{LO},0}$  varies as  $\ln \epsilon_F$  according to Eq. 17. Another KA occurs when the Fermi energy reaches the minimum of the second bands  $E_{11}^M/2 = 0.83 \text{ eV}$ . This second KA is much stronger than that at  $\epsilon_F = 0$ , in agreement with Eq. 22 which predicts a variation going as  $-1/\sqrt{\epsilon_F^2 - (E_{11}^M/2)^2}$ . A frequency drop of about  $40 \text{ cm}^{-1}$ , with respect to zero doping, was reported in a theoretical calculation of alkali-doped SWNTs<sup>29</sup> at a doping level of about  $N_{el}/C \sim 0.02$ , in good agreement with our results (see Fig. 1). Other KAs occur each time the Fermi level increases

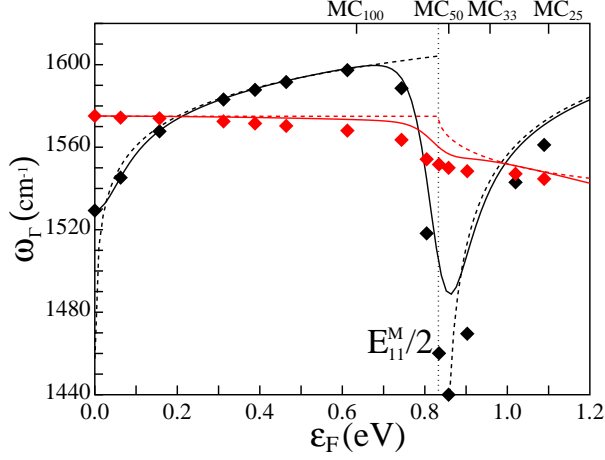


FIG. 3: (Color online) Variation, within the adiabatic approximation, of the LO axial (black) and TO tangential (red)  $\Gamma$  frequencies with the Fermi level at  $T=315$  K, calculated from DFT phonon-EZF (full diamonds), from the integral model (solid line, Eq. 11), and from the analytical model at  $T=0$  K (dashed line, Eqs. 17, 22, and 23). The metal/carbon composition corresponding to the Fermi level is indicated on the top of the figure.

such that a new conduction band is populated. In TO tangential modes, due to the vanishing of the EPC interband matrix element, the first band does not give rise to a KA; the curve is practically flat until  $E_{11}^M/2$ . The effect of the second conduction band induces a variation going as  $-\sqrt{\epsilon_F^2 - (E_{11}^M/2)^2}$  (Eq. 23).

However, as we will see in the following section, although the physics described by these results seems very intriguing, the main outcome of this comparison is the accuracy of the integral model, with respect to full DFT calculations, in predicting the Raman properties of SWNTs, and in particular the anomalous doping dependence of the vibrational axial mode.

#### IV. NON-ADIABATICITY

##### A. Time-dependent perturbation theory

The vast majority, if not the totality, of *ab initio* phonon calculations rely on the so-called Born-Oppenheimer adiabatic approximation. In this framework one can decouple the electron motion from the ion dynamics, on the basis of their large mass and velocity difference, and thus treat the electronic properties as they were completely independent of the ionic motion. This approximation for phonon calculation is equivalent to first-order time-independent perturbation theory and is wholly justified for insulators and semiconductors. Even in ordinary metals a proper, specific treatment of the electronic degrees of freedom, such the inclusion of a finite Fermi-Dirac electronic temperature, usually suffices to avoid a failure of the BO approximation.

Metallic SWNTs do however represent an “extraordinary”

case, due to their intrinsic one-dimensional nature, and the use of the adiabatic BO approximation leads to significant deviations from experimental results. This could be particularly true in the case of Raman scattering where a sinusoidal excitation induces the oscillatory motion of ions. In order to check whether a proper inclusion of non-adiabaticity would affect our previous results, we introduce a non-adiabatic model, based on time-dependent perturbation theory. In the process of absorption and emission of a phonon by the electrons, the phonon energy is no longer neglected: we replace, in Eq. 11, the energy difference between the two electronic scattering states,  $(\epsilon_{\mathbf{k},i} - \epsilon_{\mathbf{k}+\mathbf{q},f})$ , by  $(\epsilon_{\mathbf{k},i} - \epsilon_{\mathbf{k}+\mathbf{q},f} + \hbar\omega_{\mathbf{q}} + i\delta)$ . Here we add a small imaginary part  $\delta$  to the energy to control the divergences. Eq. 11 then becomes:

$$\tilde{D}_{\mathbf{q}}^{\text{TO/LO}} = \frac{a_0^2 \sqrt{3} \langle G_{\Gamma}^2 \rangle_{\text{F}}}{\pi^2 d} \sum_{\nu, f, i} \int_{-\bar{k}}^{\bar{k}} dk' \frac{f[\epsilon_{\nu, i}(k')] - f[\epsilon_{\nu, f}(k' + q)]}{\epsilon_{\nu, i}(k') - \epsilon_{\nu, f}(k' + q) + \hbar\omega_{\mathbf{q}} + i\delta} \quad (25)$$

The frequency is obtained as  $\omega_{\mathbf{q}} = \sqrt{\frac{\Re(D_{\mathbf{q}})}{M}}$ , that is, we take the principal part of the above integral by letting  $\delta \rightarrow 0$ . Since  $D_{\mathbf{q}}$  depends on the frequency, this equation should be solved self-consistently.

In the  $\mathbf{q} \rightarrow 0$  limit, Eq. 12 then becomes, in the NA case,

$$\tilde{D}_{\Gamma}^{\text{TO/LO}} = \frac{a_0^2 \sqrt{3} \langle G_{\Gamma}^2 \rangle_{\text{F}}}{\pi^2 d} \int_{-\bar{k}}^{\bar{k}} dk' \left\{ \sum_{\nu, f \neq i} \frac{f[\epsilon_{\nu, i}(k')] - f[\epsilon_{\nu, f}(k')]}{\epsilon_{\nu, i}(k') - \epsilon_{\nu, f}(k') + \hbar\omega_{\Gamma} + i\delta} \right\} \quad (26)$$

Here only the interband transitions contribute to the dynamical matrix, since, for an optical phonon, the limit

$$\lim_{\mathbf{q} \rightarrow 0} \frac{f[\epsilon_{\nu, f}(k')] - f[\epsilon_{\nu, f}(k' + q)]}{\epsilon_{\nu, f}(k') - \epsilon_{\nu, f}(k' + q) + \hbar\omega_{\mathbf{q}} + i\delta} = 0 \quad (27)$$

We can anticipate that the absence of the intraband contributions dramatically affects the results when such terms are important, *i.e.* when the Fermi level is close to a  $E_{\nu\nu}^M/2$  band minimum. As in the previous section, we study the contribution of the  $\nu = 0, \pm 1$  bands to the non-analytical part of the dynamical matrix. The mode frequencies are obtained from the dynamical matrix as in Eq. 24.

##### B. Contribution of the $\nu = 0$ bands

Eq. 26 can be integrated, by using linear bands and  $T = 0$ , analogously to the calculations developed in the static case; we thus obtain for the non-analytical part of  $D_{\Gamma}$  in the case of LO axial phonons

$$\tilde{D}_{\Gamma}^{\text{LO}, 0} = \frac{2a_0^2 \sqrt{3}}{\pi^2 d \beta} \langle G_{\Gamma}^2 \rangle_{\text{F}} \ln \frac{|2\epsilon_F + \hbar\omega_{\Gamma}^{\text{LO}}| |2\epsilon_F - \hbar\omega_{\Gamma}^{\text{LO}}|}{|2\beta \bar{k}|^2} \quad (28)$$

while the TO tangential term  $\tilde{D}_{\Gamma}^{\text{TO}, 0}$  is zero since it involves the intraband terms only. We note that the KA observed in the static case for zero doping is replaced by two logarithmic divergences at a doping level  $\epsilon_F = \pm \hbar\omega_{\Gamma}^{\text{LO}}/2$ , which is  $N_{el}/C \approx 0.0015$  ( $\sim \text{MC}_{650}$ ). As shown schematically in

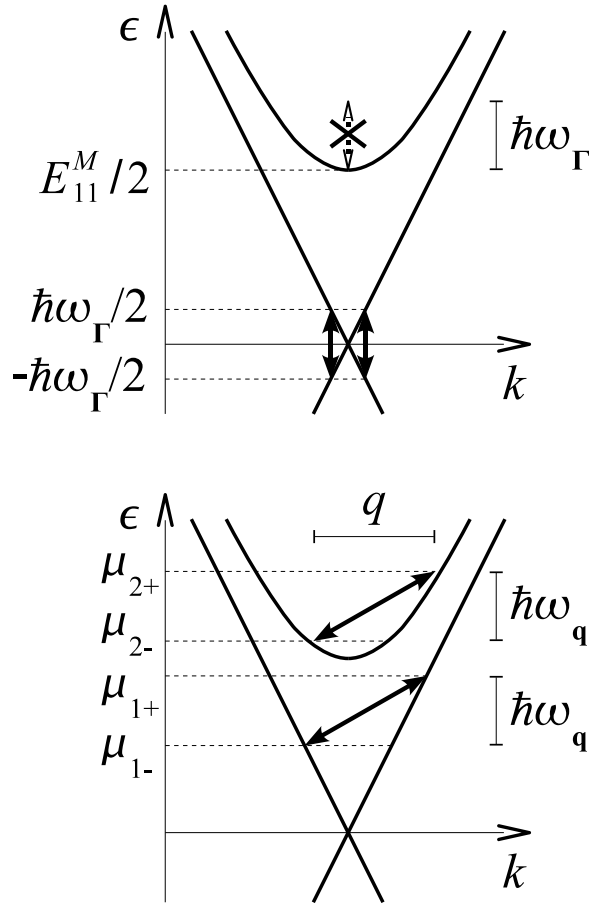


FIG. 4: Schematic representation of electronic transitions allowed by conservation of energy and momentum in electron-phonon scattering processes involving a phonon with momentum  $\mathbf{q}$  and energy  $\hbar\omega_{\mathbf{q}}$ . An abrupt change in the phonon dispersion, *i.e.* a Kohn anomaly, occurs when, by change of the Fermi energy, one of this transitions becomes allowed or forbidden by the Pauli exclusion principle. In practice, this occurs when the Fermi level crosses a tip of one of the arrows corresponding to allowed transitions. Top panel: transitions at  $\mathbf{q}=\mathbf{0}$  ( $\Gamma$ ). Bottom panel: transitions at a finite  $\mathbf{q}$ -point.

the top panel of Fig. 4,  $\Gamma$  transitions conserving energy and momentum in the scattering process can indeed occur when connecting two bands separated by an energy equal to  $\hbar\omega_{\Gamma}$ , which is in practice the case only in correspondence of the electronic vertical transitions ( $\mathbf{q}=\mathbf{0}$ ) between the  $\pi$  and the  $\pi^*$  bands.

### C. Contribution of the $|\nu| \geq 1$ bands

The effect of the non-adiabatic terms in the  $\nu = 0$  bands contribution merely consists in a splitting of the zero-doping Kohn anomaly observed in the static case. The picture changes completely for the  $|\nu| \geq 1$  bands. In fact, given the energy gap between the  $\pi$  and  $\pi^*$  bands having  $\nu \neq 0$ , only the intraband terms are relevant to Kohn anomalies. These intra-

band terms are suppressed by the dynamical effects (Eq. 26) in both LO and TO modes and thus  $\tilde{D}_{\Gamma}^{\text{LO,TO},\nu \neq 0} = 0$ . Indeed in the hyperbolic band it is not possible to conserve both energy and momentum in an electron-phonon scattering process with a  $\mathbf{q} = 0$  optical phonon, see Fig. 4. In addition to the analytical calculation at  $T=0$ , we performed numerical integrations of Eq. 26 at different temperatures (77 K, 315 K). As in the static case, we used polynomial fits to describe the band dispersions. We report in Fig. 5 the variation of the LO axial mode as function of the Fermi level in the non-adiabatic case at those two temperatures. The results are consistent with the analytical ones obtained at vanishing temperature; the only Kohn anomaly is observed, as explained in the previous subsection, at  $\hbar\omega_{\Gamma}/2$ . All the other Kohn anomalies, that in the adiabatic approximation and thus in all standard DFT calculations are due to the population of new energy levels, completely disappear. This is a general behavior for vertical transitions.

### D. LO phonon linewidth

An important measurable quantity is the phonon linewidth. In ref.<sup>24</sup> it is shown that it can be split into a EPC direct contribution, only relevant in metallic nanotubes, and a term due to inhomogeneous broadening and anharmonicities, common to all nanotubes and estimated around  $10 \text{ cm}^{-1}$  from experimental data. The LO axial phonon linewidth (full width at half maximum)  $\gamma_{\text{LO}}^{\text{EPC}}$  as function of the electronic doping can instead be calculated<sup>39</sup> from the imaginary part of the non-adiabatic dynamical matrix, Eq. 25, as  $\gamma_{\mathbf{q}} = |\Im(\tilde{D}_{\mathbf{q}})|/(\omega_{\mathbf{q}}M)$ . An identical result is obtained by using the Fermi golden rule, as in ref.<sup>24</sup>. The result of ref.<sup>24</sup> derived in nanotubes for zero doping can be easily generalized for any doping as:

$$\begin{aligned} \gamma_{\text{LO}}^{\text{EPC}}(\epsilon_F) &= \frac{2a_0^2\sqrt{3}}{\pi d\beta M\omega_{\Gamma}^{\text{LO}}} \langle G_{\Gamma}^2 \rangle_{\text{F}} \left[ \frac{1}{e^{(\epsilon_F - \hbar\omega_{\Gamma}^{\text{LO}}/2)/k_B T} + 1} - \frac{1}{e^{(\epsilon_F + \hbar\omega_{\Gamma}^{\text{LO}}/2)/k_B T} + 1} \right] \\ &= \frac{79 \text{ cm}^{-1} \text{ nm}}{d} \left[ \frac{1}{e^{(\epsilon_F - \hbar\omega_{\Gamma}^{\text{LO}}/2)/k_B T} + 1} - \frac{1}{e^{(\epsilon_F + \hbar\omega_{\Gamma}^{\text{LO}}/2)/k_B T} + 1} \right] \end{aligned}$$

At zero doping this FWHM equals, at  $T=315 \text{ K}$ , about  $60 \text{ cm}^{-1}$  for a (9,9) SWNT. We show the EPC LO linewidth in the top panel of Fig. 5. At  $T \rightarrow 0$  this term is constant up to the Kohn anomaly at a  $N_{el}/C \approx 0.0015$  (MC<sub>650</sub>) doping level, and vanishes abruptly for higher doping levels, while a smoother behavior is observed at finite temperature. Since all the terms contributing to the EPC part of the dynamical matrix vanish for the TO tangential modes, the corresponding phonon linewidth will vanish as well.

### E. Finite-q results

In the previous subsections, we have developed our analytical model at the  $\Gamma$  point of the Brillouin zone, and we have shown that the proper treatment of non-adiabatic terms lifts



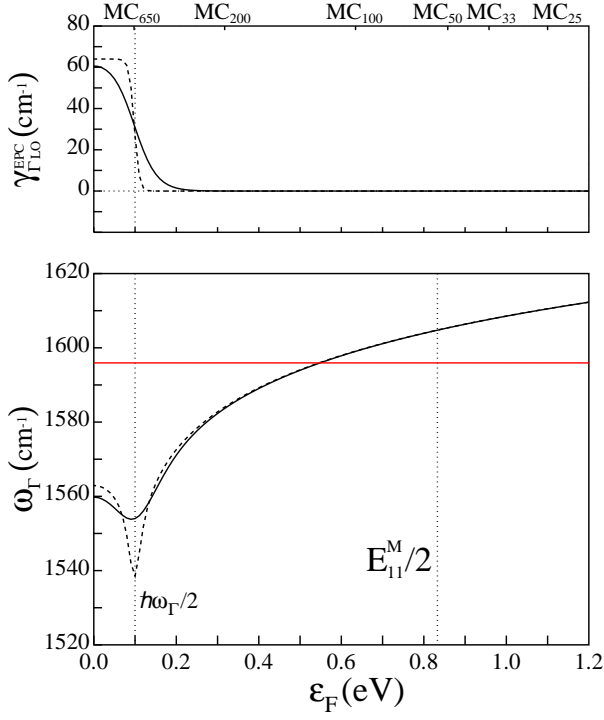


FIG. 5: (Color online) Lower panel: variation of the LO axial ( $G^-$  peak in Raman experiments, black) and TO tangential ( $G^+$  peak, red)  $\Gamma$  frequencies with the Fermi level at  $T=315$  K (solid line) and at 77 K (LO axial, dashed line), calculated from the **non-adiabatic** integral model (Eq. 25). Top panel: variation, at the same temperatures, of the EPC contribution to the FWHM of the LO axial mode with the doping level. The metal/carbon composition corresponding to the Fermi level is indicated on the top of the figure.

all the divergences resulting from intraband, vertical transitions. However, as shown schematically in the lower panel of Fig. 4, at finite  $\mathbf{q}$  the outcome is different from the  $\Gamma$  case. Indeed, non-vertical intraband transitions conserving energy and momentum can occur when  $\mathbf{q}$  is approximately larger than  $\omega_q/v_M$ ,  $v_M$  being the maximum electronic band velocity. We report in Fig. 6 the dependence on electronic doping of the LO axial frequency at  $\mathbf{q}=0.05 \cdot \frac{2\pi}{a_0}$  and  $0.1 \cdot \frac{2\pi}{a_0}$ , calculated numerically through Eq. 25 at  $T=77$  K and 315 K. In this case the intraband Kohn anomalies observed in the adiabatic approximation are not suppressed, as it is the case for vertical transitions. The interband KA is shifted towards higher doping levels with respect to the  $\Gamma$  case. The intraband KAs are shifted in the same direction with respect to the energy levels  $E_{\nu\nu}^M/2$ . Both interband and intraband Kohn anomalies appear in doublets, separated by  $\hbar\omega_q$ .

By using the expressions for EPC derived in Refs.<sup>34,38</sup> for the scattering involving phonons near the  $\mathbf{K}$  point, it can be shown that the behavior of the highest optical phonon at a wavevector  $\mathbf{q}+\mathbf{K}$  is very similar to the one reported in Fig. 6 for the LO axial frequency at  $\mathbf{q}$ . This phonon near the  $\mathbf{K}$  point is responsible for the  $D$  band observed experimentally in Raman spectra.

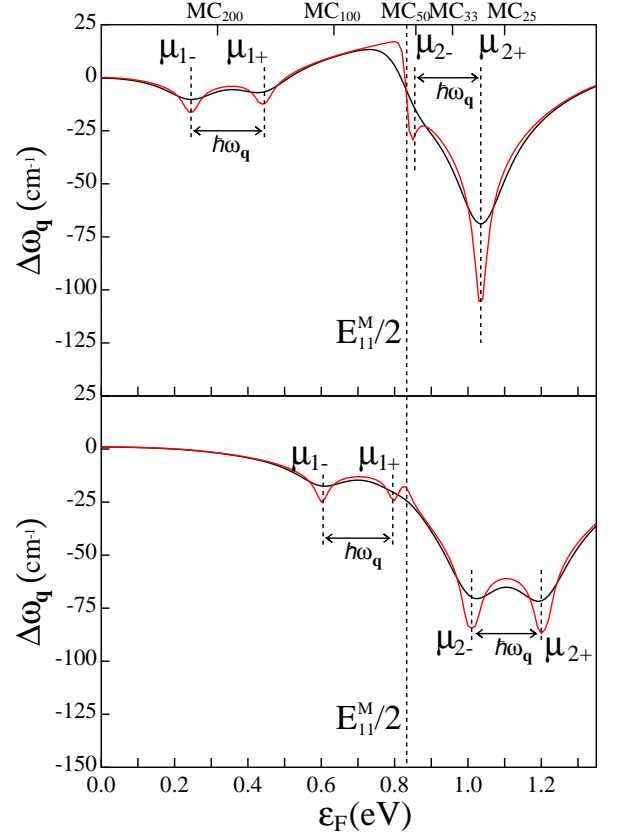


FIG. 6: (Color online) Lower panel: variation, with respect to zero doping, of the LO axial frequencies with the Fermi level at  $T=315$  K (black) and  $T=77$  K (red), calculated from the **non-adiabatic** integral model (Eq. 25). The phonon momentum is equal to  $\mathbf{q}=0.1 \cdot \frac{2\pi}{a_0}$ . Top panel: same, at  $\mathbf{q}=0.05 \cdot \frac{2\pi}{a_0}$ . The dotted vertical line indicates the minimum of the second conduction band. The energy values  $\mu_{1-}$ ,  $\mu_{1+}$ ,  $\mu_{2-}$ , and  $\mu_{2+}$  correspond to the levels schematically shown in Fig. 4. A similar behavior is expected for the highest optical phonon near the  $\mathbf{K}$  point, which is responsible for the Raman  $D$  band. The metal/carbon composition corresponding to the Fermi level is indicated on the top of the figure.

## V. DISCUSSION

### A. Physical properties of metallic nanotubes

In this work we presented a combination of *ab initio* DFT calculations with an integral and analytical model developed to take into account in a simple way the direct EPC contribution to the dynamical matrix, responsible for the divergences originating the KAs. Since however the mathematics behind our models might be cumbersome, here we summarize the most interesting *physical* properties of metallic SWNTs we observe, as well as the quantitative results on experimentally measurable quantities.

We showed that KAs in SWNTs can be identified by considering electron-phonon scattering processes that conserve both energy and momentum (see Fig. 4 and relative discus-

sion). Since there are strong disagreements between the adiabatic and the non-adiabatic case, only the results obtained through the latter model are reliable. The failure of the adiabatic calculation originates from the fact that, in this approximation, the phonon energy is neglected and the energy conservation in the electron-phonon scattering processes is thus violated. Since the curves shown in Figs. 1 and 3 are obtained through the adiabatic model and through DFT frozen-phonon and DFPT calculations, those results should not be used for comparison to experimental data. On the other hand, all the results presented in Figs. 5 and 6, which conflict with any existing DFT calculation based on the BO approximation, are in principle *correct*, and are thus meant to be directly compared to experiments.

The results shown in Fig. 5 promise to be useful tools to determine experimentally the doping level of individual metallic SWNTs. In particular, by measuring the shift of the  $G^-$  peak with respect to zero doping and its linewidth, one can determine the variation of the Fermi energy and thus the doping level. Those results refer to a (9,9) nanotube of diameter 1.23 nm; however, they can be easily generalized to any  $d$ -diameter metallic SWNT by observing that the dependence of both the linewidth of the  $G^-$  peak and its frequency shift with respect to zero doping case are proportional to  $1/d$  and independent of the chirality. We note here that we are assuming that the  $G$  peak originates from single resonance.

It was showed that carbon nanotubes<sup>36,37</sup>, as graphite<sup>40,41</sup>, present a free-electron-like interlayer state whose energy level decreases rapidly with increasing doping, and reaches the Fermi energy at about the saturation doping of  $\sim MC_8$ . We showed that KAs occur at  $\Gamma$  only when the Fermi energy is in proximity of a band crossing with non-zero interband electron-phonon coupling. Besides the crossing of the  $\pi$ -bands at zero doping, we estimate that the first band-crossing with symmetry-allowed transitions is that between the interlayer level and the  $\pi^*$  ( $\nu = 0$ ) bands. Such crossing is a candidate for a Kohn anomaly. This could explain the strong softening of about  $50 \text{ cm}^{-1}$  observed at saturation doping in experimental Raman studies on the  $G$  peak in alkali-doped SWNTs<sup>5,42</sup>.

Finally, we predicted KAs to occur in phonons with *finite* momentum  $\mathbf{q}$  not only in proximity of a band crossing, but also each time a new band is populated (see Fig. 6). Therefore, by experimentally probing such KAs, the filling of the hyperbolic bands could be detected. Phonons at finite- $\mathbf{q}$  vectors are experimentally accessible to double-resonant Raman scattering<sup>43</sup>, and correspond in the Raman spectra, *e.g.*, to the defect-activated  $D$  peak at about  $1350 \text{ cm}^{-1}$ , and to the second-order (two-phonon)  $2D$  and  $2G$  peaks at approximately  $2700$  and  $3200 \text{ cm}^{-1}$ . We showed in Fig. 6 the variation of the phonon frequency with respect to doping at  $\mathbf{q}=0.05 \cdot \frac{2\pi}{a_0}$  and  $0.1 \cdot \frac{2\pi}{a_0}$ . These phonon momenta are experimentally accessible to double-resonant Raman scattering<sup>19</sup>.

Although our computational study has been limited to a

metallic SWNT, our analytical results allow to predict the behavior of the high-energy Raman peaks in semiconducting nanotubes. Since in this case only intraband terms contribute to the EPC term of the dynamical matrix, we expect the  $G$  peak to be unaffected by electron doping. On the other hand, analogously to the metallic case, the defect-activated  $D$  peak should be sensitive to doping, provided that the excitation energy is sufficient to populate the first excited electronic level in the conduction band.

## B. Conclusions

In this work we presented a theoretical study on the vibrational/Raman properties of electron-doped SWNTs using Density-Functional Theory and analytical models. We performed our calculations within the adiabatic Born-Oppenheimer approximation, but we also used time-dependent perturbation theory to explore non-adiabatic effects beyond this approximation. We showed that the Born-Oppenheimer approximation, predicts, for increasing doping levels, a series of EPC-induced KAs in the vibrational mode parallel to the tube axis at the  $\Gamma$  point of the Brillouin zone, usually indicated in Raman spectroscopy as the  $G^-$  peak. Such Kohn anomalies would arise each time a new conduction band is populated. However, we showed that they are an artifact of the adiabatic approximation, which is the standard approach for ab-initio phonon calculations. The inclusion of non-adiabatic effects dramatically affects the results, predicting KAs at  $\Gamma$  only when  $\epsilon_F$  is close to a band crossing  $E_X$ . For each band crossing a double KA occurs for  $\epsilon_F = E_X \pm \hbar\omega/2$ , where  $\hbar\omega$  is the phonon energy. In particular, for a 1.2 nm metallic nanotube, we predicted a KA to occur in the so-called  $G^-$  peak at a doping level of about  $N_{el}/C = \pm 0.0015$  atom ( $\epsilon_F \approx \pm 0.1 \text{ eV}$ ) and, possibly, close to the saturation doping level ( $N_{el}/C \sim 0.125$ ), where an interlayer band crosses the  $\pi^*$  nanotube bands. Furthermore, we predicted that the Raman linewidth of the  $G^-$  peak significantly decreases for  $|\epsilon_F| \geq \hbar\omega/2$ . Thus our results provide a tool to determine experimentally the doping level from the value of the frequency shift and from the linewidth of the  $G^-$  peak. Finally, we predicted Kohn anomalies to occur in phonons with finite momentum  $\mathbf{q}$  not only in proximity of a band crossing, but also each time a new band is populated. Such Kohn anomalies should be observable in the double-resonant Raman peaks, such as the defect-activated  $D$  and peak, and the second-order peaks  $2D$  and  $2G$ . We also predict that in semiconducting nanotubes the  $G$  peak should be insensitive to doping, while the  $D$  peak should be affected analogously to the metallic case.

We thank N. Bendiab, S. Piscanec and A. C. Ferrari for useful discussions. DFT calculations have been performed at the IDRIS French National Computational Facility under the projet CP9-61387.

\* Electronic address: saitta@impmc.jussieu.fr

<sup>1</sup> S. Iijima, Nature **354**, 56 (1991).

- <sup>2</sup> R. Saito, G. Dresselhaus, and M. S. Dresselhaus, *Physical properties of carbon nanotubes* (Imperial College Press, 1998).
- <sup>3</sup> S. Reich, C. Thomsen, and J. Maultzsch, *Carbon nanotubes : basic concepts and physical properties* (Wiley-VCH, 2004).
- <sup>4</sup> J. T. Ye, Z. M. Li, Z. K. Tang, and R. Saito, Phys. Rev. B **67**, 113404 (2003).
- <sup>5</sup> N. Bendiab, L. Spina, A. Zahab, P. Poncharal, C. Marliere, J.-L. Bantignies, E. Anglaret, and J.-L. Sauvajol, Phys. Rev. B **63**, 153407 (2001).
- <sup>6</sup> N. Bendiab, E. Anglaret, J.-L. Bantignies, A. Zahab, J.-L. Sauvajol, P. Petit, C. Mathis, and S. Lefrant, Phys. Rev. B **64**, 245424 (2001).
- <sup>7</sup> N. Bendiab, A. Righi, E. Anglaret, J.-L. Sauvajol, L. Duclaux, and F. Beguin, Chem. Phys. Lett. **339**, 305 (2001).
- <sup>8</sup> N. Bendiab, *Structure et vibrations des nanotubes de carbone intercalés* (2003), thesis, Université Montpellier II.
- <sup>9</sup> G. Chen, C. A. Furtado, U. J. Kim, and P. C. Eklund, Phys. Rev. B **72**, 155406 (2005).
- <sup>10</sup> V. Meunier, J. Kephart, C. Roland, and J. Bernholc, Phys. Rev. Lett. **88**, 075506 (2002).
- <sup>11</sup> X. Liu, T. Pichler, M. Knupfer, and J. Fink, Phys. Rev. B **67**, 125403 (2003).
- <sup>12</sup> H. Rauf, T. Pichler, M. Knupfer, J. Fink, and H. Kataura, Phys. Rev. Lett. **93**, 096805 (2004).
- <sup>13</sup> J.-L. Bantignies, L. Alvarez, R. Aznar, L. Almairac, J.-L. Sauvajol, L. Duclaux, and F. Villain, Phys. Rev. B **71**, 195419 (2005).
- <sup>14</sup> P. Corio, A. Jorio, N. Demir, and M. S. Dresselhaus, Chem. Phys. Lett. **392**, 396 (2004).
- <sup>15</sup> S. B. Cronin *et al.*, Appl. Phys. Lett. **84**, 2052 (2004).
- <sup>16</sup> P. M. Rafailov, J. Maultzsch, and C. Thomsen, Phys. Rev. B **72**, 045411 (2005).
- <sup>17</sup> Z. Wang, H. Pedrosa, T. Krauss, and L. Rothberg, Phys. Rev. Lett. **96**, 047403 (2006).
- <sup>18</sup> J. Maultzsch, S. Reich, and C. Thomsen, Phys. Rev. B **65**, 233402 (2002).
- <sup>19</sup> J. Maultzsch, S. Reich, U. Schlecht, and C. Thomsen, Phys. Rev. Lett. **91**, 087402 (2003).
- <sup>20</sup> J. Maultzsch, H. Telg, S. Reich, and C. Thomsen, Phys. Rev. B **72**, 205438 (2005).
- <sup>21</sup> H. Son *et al.*, Phys. Rev. B **74**, 073406 (2006).
- <sup>22</sup> A. Jorio *et al.*, Phys. Rev. B **62**, 115411 (2002).
- <sup>23</sup> A. Jorio *et al.*, Phys. Rev. B **71**, 075401 (2005).
- <sup>24</sup> M. Lazzeri, S. Piscanec, F. Mauri, A. C. Ferrari, and J. Robertson, Phys. Rev. B **73**, 155426 (2006).
- <sup>25</sup> S. Piscanec, M. Lazzeri, J. Robertson, A. C. Ferrari, and F. Mauri (2006), cond-mat/0611693.
- <sup>26</sup> V. N. Popov and P. Lambin, Phys. Rev. B **73**, 085407 (2006).
- <sup>27</sup> O. Dubay, G. Kresse, and H. Kuzmany, Phys. Rev. Lett. **88**, 235506 (2002).
- <sup>28</sup> O. Dubay and G. Kresse, Phys. Rev. B **67**, 035401 (2003).
- <sup>29</sup> B. Akdim, X. Duan, D. A. Shiffler, and R. Pachter, Phys. Rev. B **72**, 121402(R) (2005).
- <sup>30</sup> K.-P. Bohnen, R. Heid, H.J. Liu, and C.T. Chan, Phys. Rev. Lett. **93**, 245501 (2004).
- <sup>31</sup> D. Connétable, G.-M. Rignanese, J.-C. Charlier, and X. Blase, Phys. Rev. Lett. **94**, 015503 (2005).
- <sup>32</sup> V. Zólyomi and J. Kürti, Phys. Rev. B **70**, 085403 (2004).
- <sup>33</sup> S. Baroni, S. de Gironcoli, A. Dal Corso, and P. Giannozzi, Rev. Mod. Phys. **73**, 515 (2001).
- <sup>34</sup> S. Piscanec, M. Lazzeri, F. Mauri, A. Ferrari, and J. Robertson, Phys. Rev. Lett. **93**, 185503 (2004).
- <sup>35</sup> S. Baroni, A. Dal Corso, S. de Gironcoli, P. Giannozzi, C. Cavazzoni, G. Ballabio, S. Scandolo, G. Chiarotti, P. Focher, A. Pasquarello, *et al.*, [www.quantum-espresso.org](http://www.quantum-espresso.org).
- <sup>36</sup> E. R. Margine and V. H. Crespi, Phys. Rev. Lett. **96**, 196803 (2006).
- <sup>37</sup> J. Lu, S. Nagase, S. Zhang, and L. Peng, Phys. Rev. B **69**, 205304 (2004).
- <sup>38</sup> M. Lazzeri, S. Piscanec, F. Mauri, A. C. Ferrari, and J. Robertson, Phys. Rev. Lett. **95**, 236802 (2005).
- <sup>39</sup> W. Jones and N. H. March, *Theoretical solid state physics, Vol. 1* (Dover publications Inc., New York, 1985).
- <sup>40</sup> M. Posternak, A. Baldereschi, A. J. Freeman, E. Wimmer, and M. Weinert, Phys. Rev. Lett. **50**, 761 (1983).
- <sup>41</sup> G. Csányi, P. B. Littlewood, A. H. Nevidomskyy, C. J. Pickard, and B. D. Simons, Nature Phys. **1**, 42 (2005).
- <sup>42</sup> J.-L. Sauvajol, N. Bendiab, E. Anglaret, and P. Petit, C. R. Physique **4**, 1035 (2003).
- <sup>43</sup> C. Thomsen and S. Reich, Phys. Rev. Lett. **85**, 5214 (2000).